Heliyon 10 (2024) e37707

Contents lists available at ScienceDirect

Heliyon

journal homepage: www.cell.com/heliyon

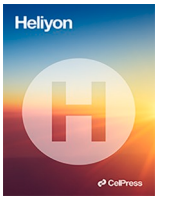

Research article

Rotator cuff repair with all-suture anchor enhances biomechanical properties and tendon-bone integration in a rabbit model

Chengxuan Yu [a,1], Luyi Sun [a,1], Han Gao [a,1], Huaixuan Sheng [a], Xinting Feng [a], Xing Yang [b], Jianbo Li [c], Qingjun Kong [c], Yuefeng Hao [b,***], Sijia Feng [a,**], Jun Chen [a,*]

[a] *Sports Medicine Institute of Fudan University, Department of Sports Medicine, Huashan Hospital, Fudan University, Shanghai, 200040, China*
[b] *Department of Orthopedics, Affiliated Suzhou Hospital of Nanjing Medical University, Suzhou, 215500, China*
[c] *Beijing Delta Medical Science & Technology Corporation, Beijing, 101102, China*

ARTICLE INFO

Keywords:
Rotator cuff tears
Rotator cuff repair
All-suture anchor
Biomechanical recovery
Tendon healing

ABSTRACT

Background: All-suture anchor (ASA) is a special type of suture anchor. It has been used to repair rotator cuff tears (RCTs). However, mechanical properties and tendon-bone integration at different time postoperatively remains to be unclear.
Methods: Mechanical testing and water contact angle measurements were conducted for ASA. *In vitro* biocompatibility was assessed using rat bone marrow stem cells (BMSCs), including live/dead cell staining and Cell Counting Kit-8 assays. ASA was implanted for rotator cuff repair (ASA group) in a New Zealand White rabbit model of RCTs, and a natural rotator cuff was used as a control (natural group). The animals were sacrificed, and tissue samples were harvested for biomechanical, radiographic, and histological analysis at 4, 8, and 12 weeks postoperatively.
Results: ASA was hydrophobic and had a strong mechanical property *in vitro*. The biocompatibility analysis showed that ASA had no effect on the viability of BMSCs. Mechanical testing *in vivo* revealed that a gradually improved failure load of ASA group was 118.0 ± 22.53N at 12 weeks postoperatively, which was recovered to the natural group. Micro-CT analysis indicated that an initial decrease in BMD and trabecular quality following ASA implantation, with a slight recovery observed at 12 weeks. Additionally, histological analysis showed the tendon-bone interface gradually integrated in the ASA group. A significant increase in tendon-bone interface scores was found from 4 weeks to 12 weeks. Tendon maturing score also improved in the ASA group, and Type I collagen content recovered to 18.58 ± 4.378 % at 12 weeks and no different from that of the natural group.
Conclusion: Rotator cuff repair with ASA in a rabbit model demonstrated the capacity to enhance biomechanical properties and tendon-bone integration.

* Corresponding author.
** Corresponding author.
*** Corresponding author.
E-mail addresses: 13913109339@163.com (Y. Hao), 815954681@qq.com (S. Feng), biochenjun@fudan.edu.cn (J. Chen).
[1] These authors contributed equally to this work.

https://doi.org/10.1016/j.heliyon.2024.e37707
Received 30 January 2024; Received in revised form 2 September 2024; Accepted 9 September 2024
Available online 13 September 2024

1. Introduction

Rotator cuff tears (RCTs) are commonly repaired through suture techniques. Suture anchors have become an integral tool in rotator cuff repair surgeries, primarily serving to anchor the tendon securely to the bone, thus establishing a robust and stable fixation point. In recent years, to address the issue of excessive bone removal associated with traditional suture anchors, a type of anchor, known as the all-suture anchor (ASA), has been developed [1]. Composed of ultra-high molecular weight polyethylene (UHMWPE) fibers, ASA offers the advantages of smaller size and softer texture, minimizing extensive damage to the bone surface [2]. It is reported that ASA has been increasingly utilized in both single-row and double-row repair surgeries [3,4]. ASA exhibits a distinct mechanical fixation mode compared to traditional suture anchors, including metal anchors, degradable anchors, and polyetheretherketone (PEEK) anchors [1,5]. It is characterized by the expansion of the anchor's diameter, which then securely lodges within the bone tunnel [6,7]. Therefore, it is vital to evaluate rotator cuff repair with ASA comprehensively.

Constant efforts have been made on the evaluation of repairing with ASA. Comparative studies on cadavers have assessed the biomechanical characteristics of ASA in repairing rotator cuff, shoulder labral and biceps tenodesis, revealing that ASA possesses biomechanical properties similar to traditional suture anchors [8–12]. Nevertheless, clinical founding also indicated the potential risks of bone tunnel enlargement associated with ASA, attributed to slight anchor movement or inflammatory reactions, have been noted during the healing process [13,14]. Current mechanical studies haven't investigated the postoperative mechanical outcomes *in vivo*. Besides, the quality of tissue healing is often indirectly inferred through symptoms, functional scoring, and Magnetic Resonance Imaging (MRI) assessments [15–18]. There is still a lack of evaluation of mechanical properties and tendon-bone integration at different time postoperatively.

In this study, ASAwas implanted to provide mechanical support for rotator cuff repair *in vivo*. Specifically, rotator cuff repaired with ASA (ASA group) was compared to natural rotator cuff (Natural group) at different time postoperatively, aiming to elucidate biomechanical, radiographic, and histological aspects of the rotator cuff healing process in a rabbit model of RCTs. The hypothesis is that rotator cuff repair with ASA could offer sustained mechanical support and tendon regeneration in rotator cuff repair.

2. Methods

2.1. Characterization of ASA

Characterization of the ASA provided insights into its appearance, structure, and fundamental material parameters. ASA, provided by Delta Medical (Model ASA13, Beijing Delta Medical Science & Technology Corporation), were 1.3 mm in size and made from UHMWPE. The ASA was sterilized using ethylene oxide. For gross morphological analysis, the ASA was placed in a stereo microscopes device (Leica M205 FA) and observed at magnifications of 7×, 40x, and 100x. The surface water contact angle of ASA was characterized by optical contact angle meter (OCA20, Dataphysics).

2.2. Cytocompatibility analysis

The results of *in vitro* biocompatibility serve as essential baseline data for the internal use of materials. Rat bone marrow stem cells (BMSCs) were isolated from Sprague Dawley (SD) rats and cultured in a complete medium consisting of Alpha-MEM (a-MEM, HyClone), 10 % heat-inactivated fetal bovine serum (FBS, Gibco), and 1 % penicillin/streptomycin (HyClone) [19]. The group co-cultured with ASA is designated as the UHMWPE group, whereas the control group is not subjected to co-culture. The anchor body of the ASA was trimmed into 1mm × 1 mm sections and immersed in 75 % ethanol for 30 min in culture dishes. They were then cut into wafers with a diameter of 1.2 cm. After ethanol removal, the wafers were air-dried for 3 h at room temperature and adhered to each well of a 24-well plate. BMSCs were then seeded at a density of 10^4 cells per well. The viability of BMSCs after 1, 3, and 5 days of culture was assessed using a Cell Counting Kit-8 (CCK-8) assay (Solabio), following the manufacturer's instructions. Absorbance at 450 nm was measured using a microplate spectrophotometer (BioTek Epoch) and the result was analyzed with Image J software. For live/dead cell staining, the same co-culturing method of BMSCs with ASA as used in the CCK-8 assay can be applied. BMSCs were stained according to the live/dead cell staining kit instructions (Solarbio); then, cells were observed and photographed under a fluorescence microscope. Six visual fields of cells were counted and analyzed with Image J software to calculate the number of live/dead cells.

2.3. Animal model of RCTs

All animal experimental and care protocols in this study were conducted in accordance with the Rules and Regulations of Research Facilities for Shanghai Jiao Tong University agricultural biological experiment practice field (No. 20230203). A total of 27 male adult New Zealand White rabbits (16 weeks old, weighing 3.0 ± 0.5 kg) with healthy and intact forelimbs were used for the *in vivo* experiments. The left shoulder was designated as the surgical ASA group, with assessments at 4, 8, and 12 weeks (9 rabbits in the ASA group at each time point), while the right shoulder served as the Natural Group control.

Successful rabbit models of rotator cuff tears were established. General anesthesia was induced using xylazine hydrochloride (0.2 mL/kg), which was subcutaneously injected into the lower back, followed by controlled propofol administration through the ear vein. The rabbits were then positioned in the lateral decubitus position after anesthesia and skin preparation. Following skin disinfection, an incision was made on the right lateral shoulder to expose the infraspinatus tendon by splitting the deltoid muscle. The infraspinatus

tendon was transected near its bone insertion using a No. 11 blade, and a 5-mm section of the tendon was removed to mimic RCTs. All fibrocartilaginous tissue at the native enthesis was cleared [20–22].

2.4. Surgical Procedure for rotator cuff repair with ASA

In the ASA group, the RCTs were repaired using ASA as previously described (Fig. 1A) [23]. After releasing the surrounding soft tissue, a 20-mm deep bone tunnel was created at the footprint's center using the K-wire supplied with the ASA kit, oriented perpendicular to the footprint (Fig. 1B and C). The ASA was then implanted into the bone tunnel, and the suture was pulled to tighten and expand the anchor, securing it inside the bone tunnel (Fig. 1D and E). The tendon stump was sutured to the bone surface using sutures provided with the anchor (Fig. 1F and G). All surgical wounds were closed using 3-0 nylon sutures (Ethicon), and post-operative care included free cage movement with unlimited access to water and food.

2.5. Biomechanical analysis

Mechanical testing of both ASA itself and the tendon-bone composite yielded data on ASA's inherent mechanical strength and the healing status of the rotator cuff. At 4, 8, and 12 weeks post-surgery (4w, 8w, 12w), three fresh infraspinatus tendon-humerus complex specimens from each group, along with three samples from the healthy side, were prepared for biomechanical testing. Surrounding muscle tissues were meticulously removed to isolate the infraspinatus tendon. The biomechanical properties were assessed using an electronic universal materials testing system (5569; Instron) [24]. A static preload of 1 N was applied for 5 min for preconditioning. Ultimate failure load testing was performed at an elongation rate of 5 mm/min, with the endpoint marked by tissue rupture or ASA pull-out. The ultimate failure load and stiffness were determined from the load-displacement curve.

2.6. Micro-CT analysis

Micro-CT analysis was utilized to evaluate bone healing in the RCTs model [25]. After euthanasia, shoulder joints were fixed in 4 % paraformaldehyde. They were then scanned with a micro-CT system (SkyScan 1272, Bruker) at a resolution of 9 μm per pixel, using a setting of 70 kV and 114 μA and a 0.5 mm aluminum filter. The region of interest (ROI) for the analysis was defined as the bone tissue encompassing the bone tunnel, extending to a radius of 3.5 mm. This ROI was chosen to comprehensively assess the bone quality and healing process. Quantitative parameters such as bone mineral density (BMD), bone volume to total volume ratio (BV/TV), trabecular number (Tb.N), trabecular separation (Tb.Sp), and trabecular thickness (Tb.Th) were measured using Bruker software. This analysis facilitated an understanding of the bone's response to the treatment and the overall effectiveness of the applied rotator cuff repair method.

2.7. Histological analysis

Histological analysis techniques enabled microscale examination of the tendon-bone interface and the condition of the infraspinatus tendon. At 4, 8, and 12w after surgery, 4 fresh specimens of the infraspinatus-humerus complex in each group as well as 4 samples from the healthy side were harvested, fixed in 4 % paraformaldehyde, decalcified in EDTA decalcifying fluid for 3 weeks, and embedded in paraffin. Samples were cut into 5um sections in the horizontal plane using a histotome (RM2016; Leica) and stained with hematoxylin and eosin, Masson and Type I collagen (Col-1, abcam). All sections were observed using an upright microscope (BX43; Olympus), and digital images were acquired using DP Manager software (Olympus). Tendon-bone healing was determined based on a previously reported scoring system assessing the cellular morphological characteristics of interface tissue, the extent of surrounding

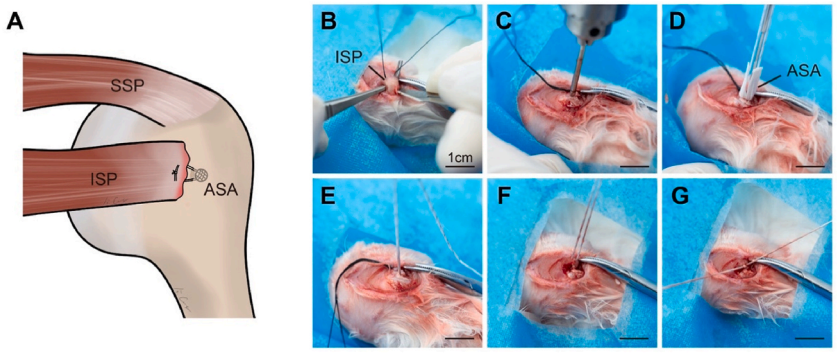

Fig. 1. Repair of Rabbit RCTs Model Using All-Suture Anchors (ASA). (A) A schematic diagram of repair of rabbit RCTs model using ASA. (B) Creation of the RCTs model by transecting the infraspinatus tendon along the bone surface. (C) Construction of bone tunnel using a K-wire. (D) Implantation of ASA into the prepared bone tunnel. (E) Tensioning and securing the ASA by pulling and tightening the suture lines. (F–G) Anchoring the tendon stump to the footprint area using the suture lines from the ASA. Scale bar = 1 cm.

fibrocartilage tissue, and the interface tissue transition from bone to tendon [26,27]. The maturation of tendon-bone tissue was evaluated using the modified tendon maturing scoring system [23,26]. Overall, 6 parameters including cellularity, proportion of cells resembling tenocytes, proportion of parallel cells, vascularity, proportion of large-diameter fibers characteristic of mature tendon fibers, and proportion of parallel fibers were evaluated semiquantitatively. ImageJ software (National Institutes of Health) was used for further quantitative analysis by an independent observer (H.G.), who was blinded to group allocation and intervention.

2.8. Statistical analysis

All data were expressed as mean ± standard deviation. Differences among groups were compared using 1-way analysis of variance with post hoc testing using the Bonferroni method. Differences between 2 groups were determined using the Student *t*-test. Statistical analysis was carried out by SPSS Statistics software (Version 21; IBM), and $P < 0.05$ was considered to be statistically significant.

3. Result

3.1. Characterization of ASA

The characterization of ASA was examined in the implanted state. As shown in Fig. 2A1-2, The anchor body was soft and deformable. The fibers of the anchor body were well-organized (Fig. 2A3-4). The suture of the ASA was also weaved by fibers (Fig. 2B1-2). The mechanical testing of ASA revealed an ultimate failure load and stiffness of 364.3 ± 18.87 N and 31.52 ± 12.72 N/mm, respectively (Fig. 2C–Table 1). The droplet of water adhered onto the surface of ASA stably (Fig. 2D). The water contact angle of the ASA was 124.5 ± 2.739°, indicating its hydrophobicity (Table 1). Overall, the ASA, weaved by well-organized fibers, has a strong mechanical property and is hydrophobic.

3.2. Biocompatibility of ASA

In vitro biocompatibility of ASA was determined by CCK-8 assay and Live/Dead cellular staining. As shown in Fig. 3A and B, no significant differences of the living cells percentages were found between blank group and ASA group at 1d, 3d, and 5d, revealed that BMSCs maintained good cell viability. Then the CCK-8 evaluated the viability of BMSCs grown with ASA from 1d to 5d (Fig. 3C). Both results showed that BMSCs in ASA group exhibited similar viability to cells in the blank group. The above analysis showed that ASA was suitable for implant *in vivo*.

3.3. Mechanical properties of Repaired Rotator Cuff Tendon

The ultimate failure load and stiffness of the tendon-bone complex were evaluated across four groups. During biomechanical testing, rupture consistently occurred near the tendon-bone interface in all groups (Fig. 4A). None of the ASA or suture was pulled out or broken. The force-displacement curves indicated that the ASA group at 12 weeks and the natural group exhibited a high failure load and a steeper curve slope, while the ASA group demonstrated the lowest maximum failure load at 4 weeks (Fig. 4B). As depicted in Fig. 4C, the data shows that there has been a steady increase to 118.0 ± 22.53N from 4 weeks to 12 weeks ($P < 0.05$). No significant differences were found between ASA group and natural group at 12 weeks ($P > 0.05$). Fig. 4D reveals that the stiffness of the tendon bone complex in ASA group was 8.546 ± 1.391N/mm at 4 weeks. A continual growth of the stiffness has been found at 8 weeks (14.72 ± 4.053N/mm), and was gradually improved to natural at 12 weeks ($P > 0.05$). The biomechanical evaluation revealed that the

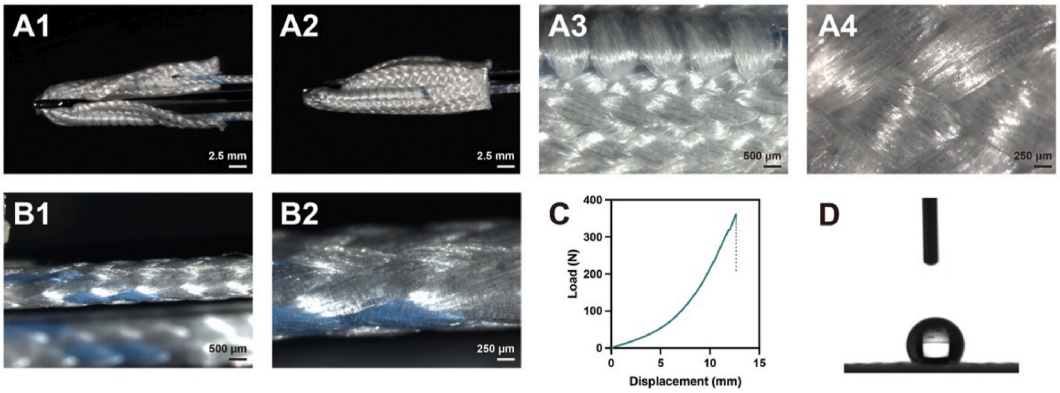

Fig. 2. Characterization of ASA. (A1-A2) Gross morphological analysis of the anchor body of the ASA. Scale bar = 2.5 mm (A3-A4) Gross morphological analysis of the fiber structure of the ASA. (A3) Scale bar = 500 μm, (A4) scale bar = 250 μm (B1-B2) Gross morphological examination of the suture material used in ASA. (C) Representative load-displacement curve demonstrating the mechanical properties of ASA. (D) Water contact angle evaluation of ASA surface.

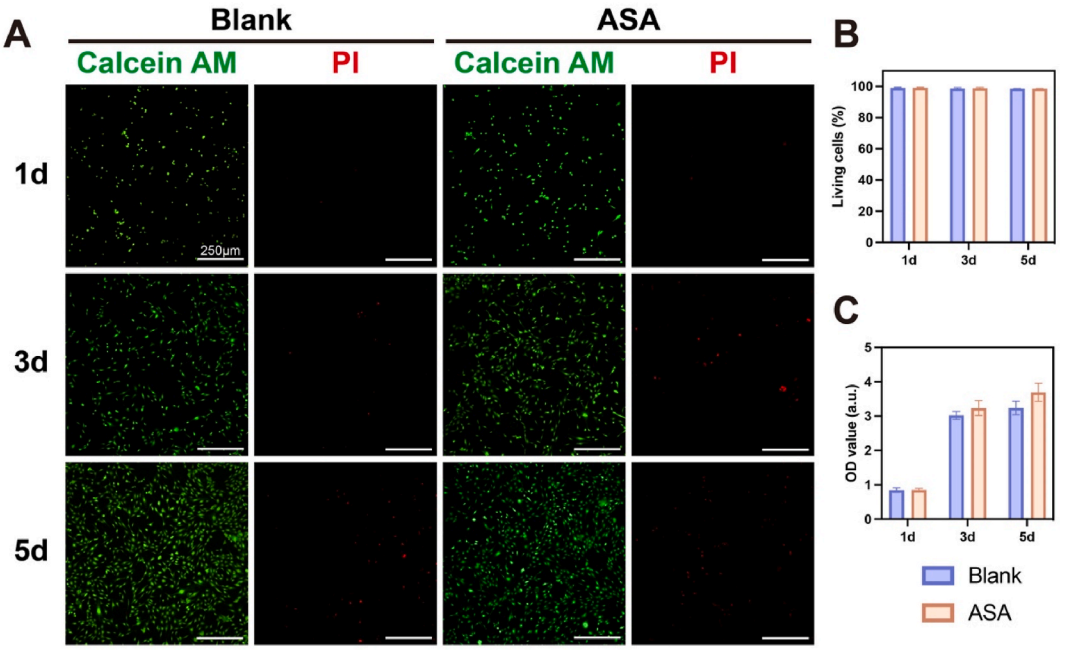

Fig. 3. The biocompatibility of ASA *in vitro*. (A) Live/Dead cellular staining of BMSCs. Scale bar = 250 μm. (B) Quantitative results of living cells. (C) Relative activity of BMSCs by CCK-8 assay. Data are shown as mean ± SD; N = 3.

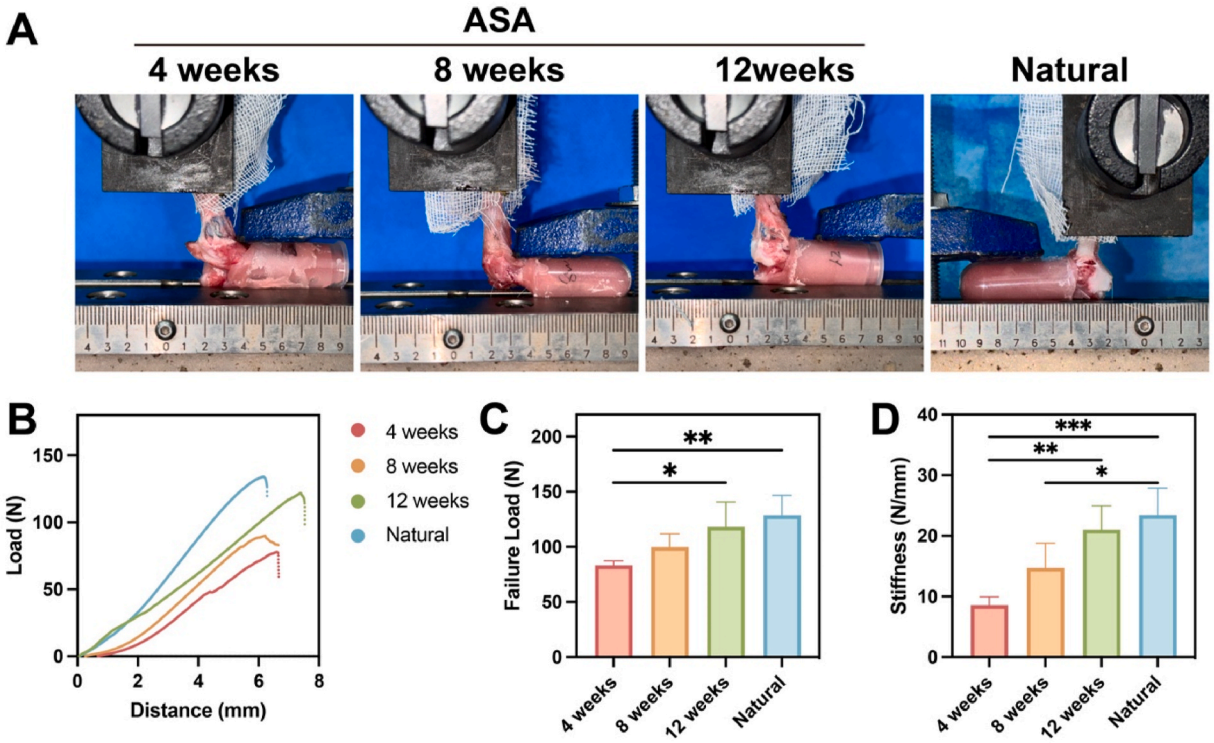

Fig. 4. Mechanical Evaluation of Repaired Rotator Cuff Tendon-Bone Complex. (A) Gross observation of tendon-bone complex failure during mechanical testing. (B) Representative load-displacement curve for the tendon-bone complex. (C–D) Failure load and stiffness in the tendon-bone complex. Data are shown as mean ± SD; N = 3; *, $P < 0.05$; **, $P < 0.01$; ***, $P < 0.001$.

Table 1
The mechanical properties of ASA[a].

Maximum Load (N)	Stiffness (N/mm)	Water Contact Angle (°)
364.3 ± 18.87	31.52 ± 12.72	124.5 ± 2.739

[a] Data are reported as mean ± SD; N = 3.

tendon-bone complex's failure load and stiffness gradually improved, indicating the recovery in mechanical properties post-repair.

3.4. Micro-CT analysis

Micro-CT analysis was utilized to evaluate bone healing in the rotator cuff repair model. After 3D reconstruction, ROI was used for analysis (Fig. 5A). At 4 weeks, 8 weeks and 12 weeks, BMD was found to be notably lower in ASA group than the natural group (Fig. 5B) ($P < 0.0001$). At 8 weeks, BV/TV decreased to 17.16 ± 4.942 % and increased from 8 weeks to 12 weeks (Fig. 5C). No significant

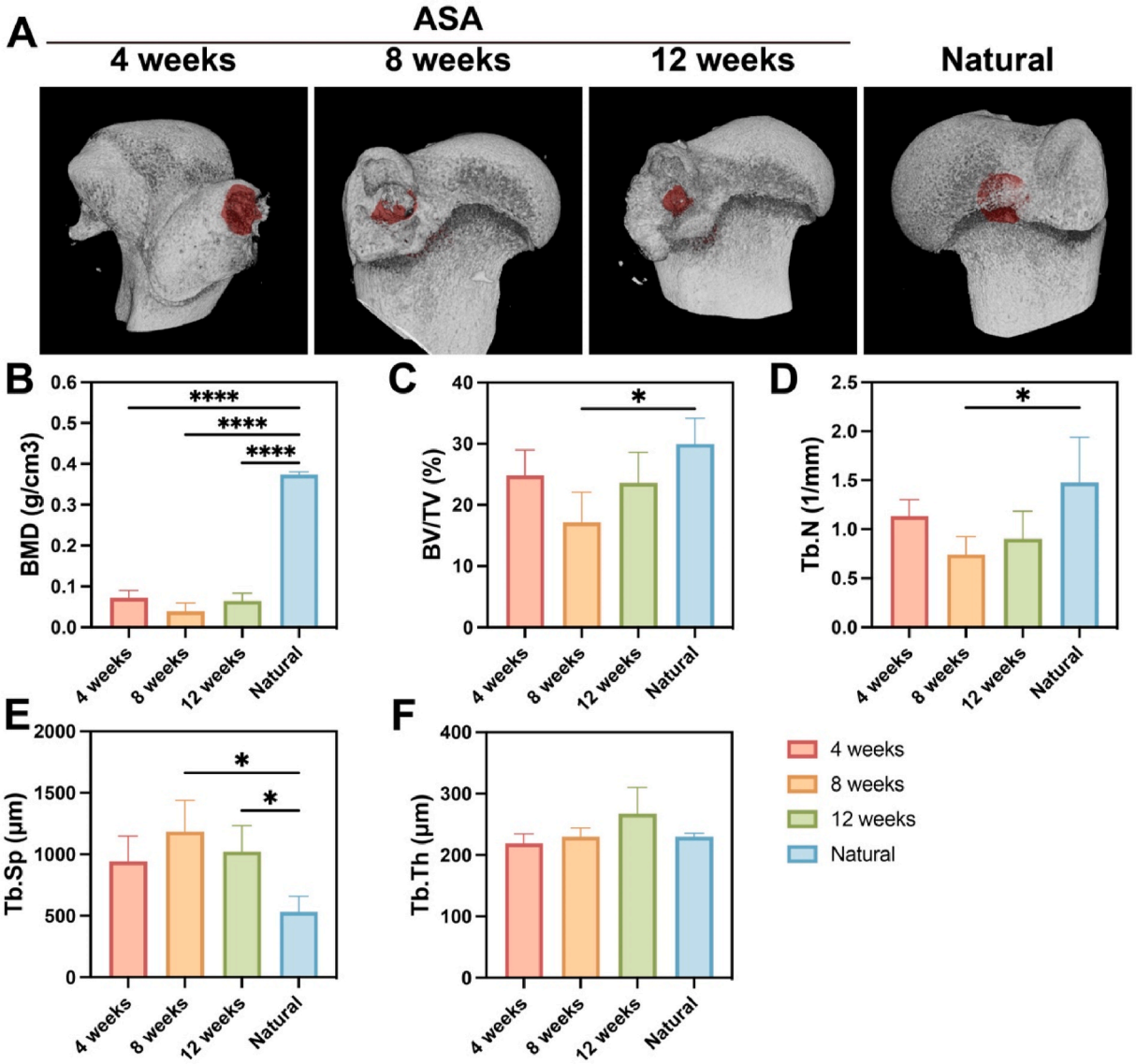

Fig. 5. Micro-CT Analysis of Bone Tunnel in Tendon-Bone Complex. (A) 3D reconstruction and cross-sectional view of the humerus in the tendon-bone complex. ROI is shown in red. (B–F) Quantitative analysis of the bone tunnel area, including bone mineral density (BMD), bone volume to tissue volume ratio (BV/TV), trabecular number (Tb.N), trabecular separation (Tb.Sp), and trabecular thickness (Tb.Th). Data are shown as mean ± SD; N = 3; *, P < 0.05; ****, P < 0.0001.

difference of BV/TV was found in ASA group compared with the natural at 12 weeks. Tb.N, Tb.Sp, Tb.Th were analyzed to indicate the quality of trabecular. After the Tb.N in ASA group declined to 0.7422 ± 0.1808/mm at 8 weeks, it began to increase and slightly lower than the natural group (Fig. 5D) ($P > 0.05$). Tb.Sp rise to 1217 ± 216.4 μm post-repair, showing a higher separation than the natural group at 8 weeks ($P < 0.05$). It decreased to 954.9 ± 219.4 μm at 12 weeks but remained notably higher than the natural group, which was 599.0 ± 170.8 μm (Fig. 5E) ($P < 0.05$). From 4 weeks to 12 weeks, Tb.Th in ASA group showed no obvious differences compared to natural (Fig. 5F). Therefore, the result of micro-CT analysis revealed an initial decrease in BMD and trabecular quality following ASA implantation, with a slight recovery observed at 12 weeks.

3.5. Histological analyses

Gross observation revealed no contracture or limitations in the shoulder's range of motion, nor any evidence of suture anchor pull-out. As depicted in Fig. 6A, there were no signs of rupture or infection in either the control or ASA group. Swelling of the infraspinatus tendon was observed at 4 weeks. The swelling alleviated and the tissue enveloping the tendon-bone junction appeared denser from 4 weeks to 8 weeks. At 12 weeks, denser, fibrous tissue was observed at the tendon-bone junction, with no evident swelling, which was similar to the natural group. Therefore, the gross observation highlights the progressive healing of tendon-bone complex in the ASA group.

As illustrated in Fig. 6B, the tendon-bone interface was analyzed using hematoxylin and eosin (HE) staining and Masson's trichrome staining. In the ASA group, the tendon and bone were connected, and a few inflammatory cells were observed at 4 weeks. The Masson's trichrome staining indicated an incomplete integration at the tendon-bone interface. At 8 weeks, the interface was widened, showing integration of tendon and bone, yet still displaying signs of inflammation and vascularization. At 12 weeks, the tendon-bone integration exhibited further expansion. An increased presence of tenocyte-like cells was observed. Tendon fibers and fibrocartilaginous tissue were arranged more orderly (Fig. 6C). The tendon-bone interface score showed a steady increase from 4 weeks to 12 weeks (Fig. 6D). At 12 weeks, the tendon-bone interface score of the ASA group was 9.0 ± 0.816, which was close to the natural score. The histological analysis of tendon-bone interface suggested the gradual integration process of the tendon-bone interface after repaired with ASA.

Histological analysis of the tendon's quality was conducted (Fig. 7A). In the ASA group, tendon fibers appeared thin and disorganized at 4 weeks, with a presence of inflammatory cells (Fig. 7B). Immunohistochemical staining showed a lower content of Col-1 than natural ($P < 0.001$). At 8 weeks, the inflammatory response had decreased, with tendon fibers appearing thicker and more organized compared to the samples at 4 weeks. The fiber diameter in the tendon remnants further increased, displaying parallel alignment similar to natural group at the 12 weeks, with no apparent inflammatory response observed. The Col-1 area increased to 18.58 ± 4.378 %, which shown no obvious difference with natural tendons ($P > 0.05$). From 4 weeks to 12 weeks, the tendon maturing score of the ASA group indicated gradual improvement of tendon maturity (Fig. 7C). As shown in Fig. 7D, the distribution area of

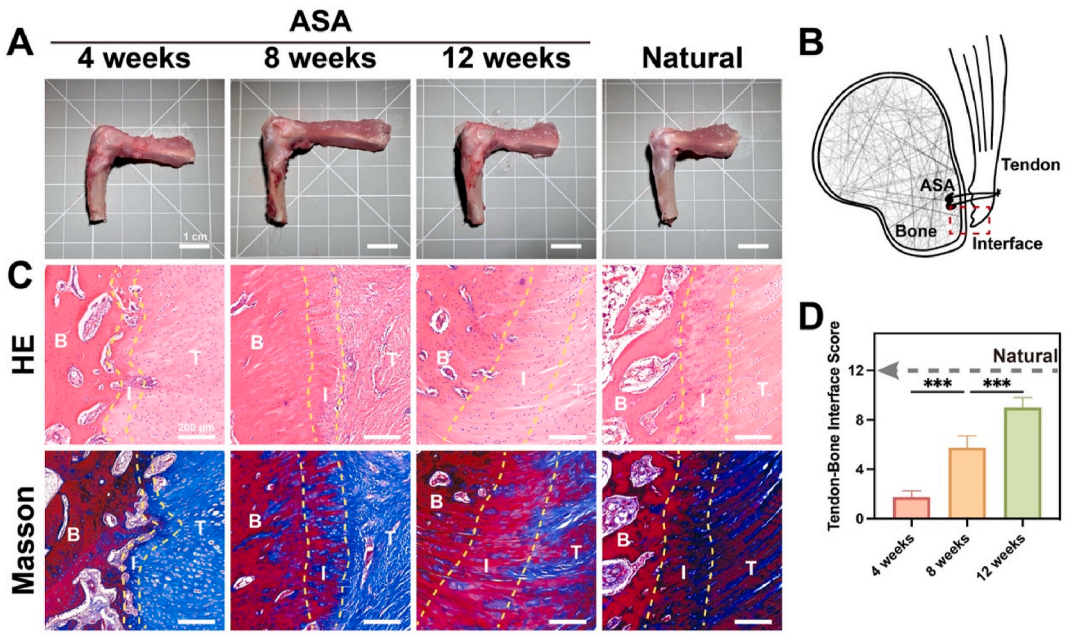

Fig. 6. Histological Analysis of Tendon-Bone Complex. (A) Macroscopic view of the tendon-bone complex. Scale bar = 1 cm. (B) Schematic representation of the tendon-bone interface. (C) Representative histological images of the tendon-bone interface, including hematoxylin and eosin staining and Masson's trichrome staining. Scale bar = 200 μm. (D) Tendon-bone interface score of the ASA groups. Labels: B, bone; I, interface; T, fibrous tissue. Data are shown as mean ± SD; N = 3; ***, P < 0.001.

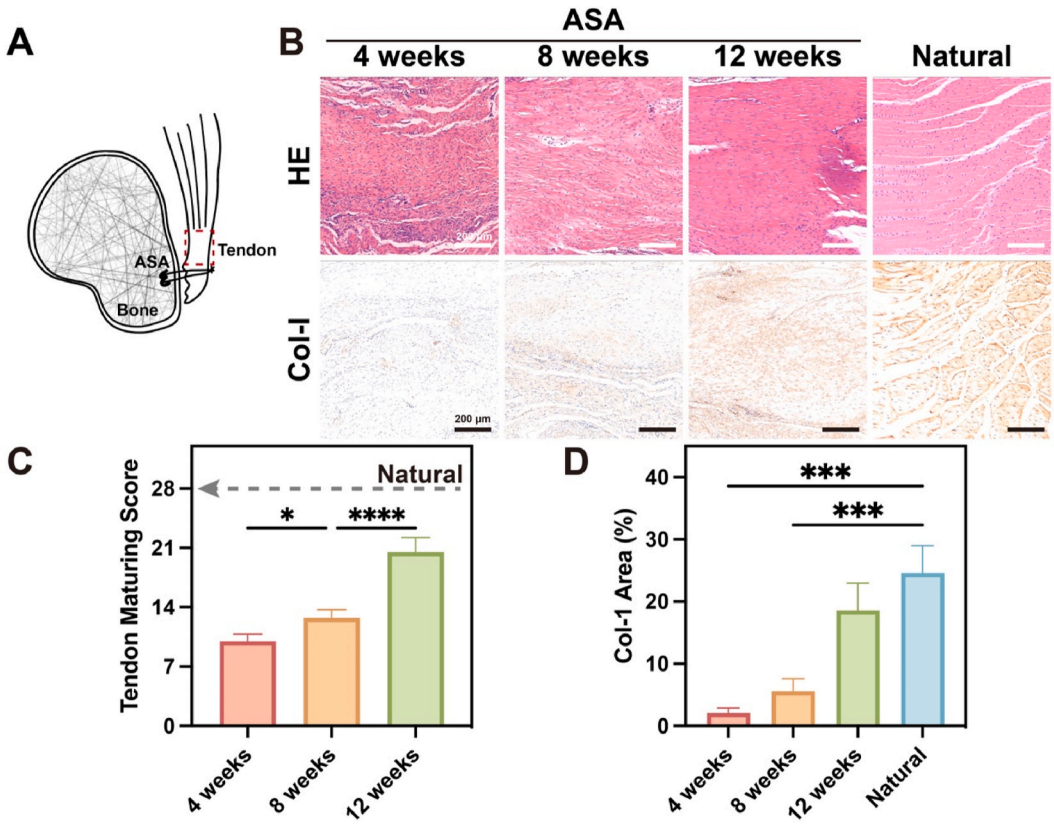

Fig. 7. Histological Analysis of Repaired Tendon. (A) Schematic representation of the tendon histology. (B) Histological images showing HE staining and collagen type I (Col-1) immunohistochemistry of the tendon. Scale bar = 200 μm. (C) Tendon maturing score. (D) Quantification of the Col-1 area in the tendon. Data are shown as mean ± SD; N = 3; *, $P < 0.05$; ***, $P < 0.001$; ****, $P < 0.0001$.

collagen fibers in the tendon remnants progressively increased. Overall, these results indicate a consistent improvement in the tendon's structural integrity and maturity from 4 weeks to 12 weeks in the ASA group.

4. Discussion

This study has shown that ASA not only restored the biomechanical properties of the repaired rotator cuff but also aided in the tendon-bone healing and tendon maturation in rabbits. Although micro-CT analysis revealed an initial decrease in bone density and trabecular quality following ASA implantation, with a recovery observed at 12 weeks, our results still point to an enhanced tendon-bone healing process. The mechanical properties and the histological analyses of the tendon-bone complex were approaching those of natural tissues at 12 weeks. These findings suggest ASA as a viable option for rotator cuff repair, warranting further exploration into their applications.

ASA maintained traditional anchor structure with a focus on minimal size and woven fibers for secure fixation [1,2,28]. It was implanted beneath the cortical bone to be fixed [29,30]. Compared to traditional suture anchors, ASA offers the advantages of smaller size and softer texture, minimizing extensive damage to the bone surface [2]. Studies affirming the biocompatibility of UHMWPE matched our findings on ASA's suitability in surgical applications, highlighting their potential to optimize outcomes and reduce complications [31]. Research has demonstrated the biocompatibility of UHMWPE, aligning with our findings on ASA's biological suitability. This highlights ASA's potential as an efficient and biocompatible solution in orthopedic surgeries.

Mechanical property is a critical parameter in evaluating anchor performance [5,32]. Several research teams have assessed the mechanical properties of commonly used all-suture anchors in the market, such as Iconix, Y-knot, and Q-Fix [33,34]. However, these studies primarily utilized cadaveric specimens, porcine cortical bone, or polyurethane foam, without considering the impact of the healing process on mechanical properties [35]. This study conducted biomechanical investigations on tendon-bone composites post-implantation of ASA for rotator cuff repair. During biomechanical testing, rupture consistently occurred near the tendon-bone interface in all groups and none of the ASA or suture was pulled out or broken. The results indicate that ASA provides essential mechanical stability necessary for rotator cuff repair. Importantly, parameters such as ultimate failure load and stiffness at the repair sites showed progressive improvement, aligning closely with the properties of natural tissue at 12w post-repair. This suggests that the mechanical environment provided by ASA not only supports initial tendon repair but also contributes to the improvement of

mechanical properties of the tendon-bone complex as the tendon matures and the tendon-bone interface heals.

Despite the compact size and soft fiber composition of ASA, concerns about their impact on the surrounding bone tunnel have been raised in orthopedic research. Studies have noted occurrences of cyst formation and bone tunnel enlargement around ASA post rotator cuff and labral repair, potentially related to micro-movements of the anchor [3,13,14,18,36,37]. In comparison to traditional suture anchors, the bone tunnel enlargement is more significant when treated with ASA(14, 38). In our study, radiological assessments were performed to analyze changes in the bone tunnel during the recovery phase post-ASA implantation. Micro-CT analysis revealed a decrease in bone density and trabecular quality at 4 and 8 weeks post-repair, characterized by reductions in BV/TV, Tb.N, and an increase in Tb.Sp. The ASA material, UHMWPE, being non-degradable with high stiffness and hydrophobic properties, may not promote bone ingrowth and could initially damage the bone tunnel, reducing both the quality and quantity of trabeculae. However, these early changes did not affect the mechanical effectiveness of ASA in the repair of RCTs, indicating that ASA can still offer reliable mechanical support for tissue repair despite these initial bone changes. The observed early postoperative decrease in bone quality also offers a basis for further advancements in anchor technology.

In this study, histological evaluations were instrumental in elucidating the process of tendon-bone healing and maturation facilitated by ASA. To our knowledge, this is the first study to histologically demonstrate the impact of ASA on the repair of RCTs. While the immediate mechanical performance of ASA post-implantation is well-documented, its long-term therapeutic effects and influence on the healing of RCTs are gaining increased attention [7,38]. Histologically, the early stages of our study revealed initial healing characterized by disorganized collagen and inflammation, which gradually evolved into more structured and mature tissue alignment. Remarkably, at 12 weeks post-repair, the tendon-bone interface exhibited well-organized collagen fibers and a reduced number of inflammatory cells, signifying advanced healing and integration. Furthermore, an increase in Col-1 content within the tendon was observed, affirming an improvement in tendon quality. These histological findings are in line with the observed trends in mechanical outcomes, indicating the role of ASA repairing in biological healing.

Considering that UHMWPE is a hydrophobic polymer short of tissue induction, it is unlikely to directly induce collagen and tendon-bone healing, as observed in this study. However, proper mechanical loading is essential for enthesis and tendon regeneration [39–41]. In previous studies on the bridging reconstruction with the hydrophobic knitted PET patch, enthesis and tendon regeneration have been found to be related to mechanical properties of the reconstruction [23]. Together, rotator cuff repair with the ASA possibly facilitated tendon-bone regeneration by improving early mechanical loading.

4.1. Limitations of the study

This study had several limitations. Firstly, the rabbit model has a few limitations common to animal studies in quadrupeds. Their gait pattern is different from humans due to the use of four limbs for weight bearing rather than two. Nonetheless, similar anatomical and biomechanical features in joints between the rabbit and human have been reported [42–44]. Secondly, this study did not directly compare ASA with other repair methods, particularly other suture anchors, in the rabbit model. Due to the limited size of the rabbit shoulder joint, it is challenging to use traditional anchors for rotator cuff repair [23,45]. Future studies will aim to use larger animal models, such as beagles and goats, to provide a more comprehensive comparison between ASA and other anchors. Thirdly, the duration of postoperative observation was limited to 12 w, restricting the scope of assessment regarding the long-term impacts of ASA implantation on bone tunnel tissues. 12w as the last time point for observation, was common in the animal studies of rotator cuff repair [45]. Future studies may extend this timeframe to provide a more comprehensive understanding.

5. Conclusion

Rotator cuff repair with ASA not only restored the biomechanical properties of the repaired rotator cuff but also aided in the tendon-bone healing and tendon maturation in rabbits, suggesting that the use of ASA could be a promising strategy for rotator cuff repair. Interestingly, a decrease in bone quality was observed early postoperative. The study highlighted the potential of ASA in clinical applications for rotator cuff repair.

Data availability

Data will be made available on request.

CRediT authorship contribution statement

Chengxuan Yu: Writing – review & editing, Writing – original draft, Methodology, Investigation, Formal analysis, Conceptualization. **Luyi Sun:** Investigation, Formal analysis. **Han Gao:** Writing – review & editing, Methodology, Investigation, Formal analysis. **Huaixuan Sheng:** Methodology, Investigation. **Xinting Feng:** Software, Resources, Formal analysis. **Xing Yang:** Validation, Investigation. **Jianbo Li:** Methodology. **Qingjun Kong:** Methodology. **Yuefeng Hao:** Writing – review & editing, Supervision. **Sijia Feng:** Writing – review & editing, Project administration, Funding acquisition, Conceptualization. **Jun Chen:** Writing – review & editing, Project administration, Funding acquisition, Conceptualization.

Declaration of competing interest

The authors declare that they have no known competing financial interests or personal relationships that could have appeared to influence the work reported in this paper.

Acknowledgments

This animal research received the approval of ethics by Shanghai Jiao Tong University agricultural biological experiment practice field (20230203). This work was supported by National Key R&D Program of China, China (2021YFA1201303), Clinical Research Plan of SHDC, Shanghai, China (SHDC2022CRT021), National Natural Science Foundation of China, China (82172511), Medical Engineering Joint Fund of Fudan University, China (YG2023-19), and Shanghai Innovative Medical Device Application Demonstration Project, Shanghai, China (23SHS00300). The authors thank from Delta Medical for providing the all-suture anchors.

References

[1] S. Chaudhry, K. Dehne, F. Hussain, A review of suture anchors, Orthopaedics and Trauma 33 (4) (2019) 263–270, https://doi.org/10.1016/j.mporth.2016.12.001.
[2] D.P. Trofa, E.C. Bixby, J.E. Fleischli, B.M. Saltzman, All-suture anchors in orthopaedic surgery: design, rationale, biomechanical data, and clinical outcomes, J. Am. Acad. Orthop. Surg. 29 (19) (2021) e950–e960, https://doi.org/10.5435/JAAOS-D-20-01224. Epub 2021/09/23. PubMed PMID: 34550098.
[3] K. Ro, S.M. Rhee, J.Y. Kim, M.S. Kim, J.D. Kim, H. Lee, et al., All-suture anchor settling after arthroscopic repair of small and medium rotator cuff tears, Am. J. Sports Med. 47 (14) (2019) 3483–3490, https://doi.org/10.1177/0363546519886547. Epub 2019/11/14. PubMed PMID: 31718248.
[4] A.M. Goschka, J.S. Hafer, K.A. Reynolds, N.S. Aberle 2nd, T.H. Baldini, M.J. Hawkins, et al., Biomechanical comparison of traditional anchors to all-suture anchors in a double-row rotator cuff repair cadaver model, Clin. Biomech. 30 (8) (2015) 808–813, https://doi.org/10.1016/j.clinbiomech.2015.06.009. Epub 2015/06/29. PubMed PMID: 26117162.
[5] L.E. Visscher, C. Jeffery, T. Gilmour, L. Anderson, G. Couzens, The history of suture anchors in orthopaedic surgery, Clin. Biomech. 61 (2019) 70–78, https://doi.org/10.1016/j.clinbiomech.2018.11.008. Epub 2018/12/07. PubMed PMID: 30502638.
[6] D. Ntalos, G. Huber, K. Sellenschloh, D. Briem, K. Puschel, M.M. Morlock, et al., Biomechanical analysis of conventional anchor revision after all-suture anchor pullout: a human cadaveric shoulder model, J. Shoulder Elbow Surg. 28 (12) (2019) 2433–2437, https://doi.org/10.1016/j.jse.2019.04.053. Epub 2019/07/18. PubMed PMID: 31311747.
[7] J.A. Ruder, E.Y. Dickinson, R.D. Peindl, N.A. Habet, J.E. Fleischli, Greater tuberosity decortication decreases load to failure of all-suture anchor constructs in rotator cuff repair, Arthroscopy 34 (10) (2018) 2777–2781, https://doi.org/10.1016/j.arthro.2018.05.030. Epub 2018/09/10. PubMed PMID: 30195950.
[8] E. Bernardoni, R.M. Frank, S.S. Veera, J.W. Griffin, B.R. Waterman, E. Shewman, et al., Biomechanical analysis of all-suture anchor fixation for rotator cuff repair, Orthop J Sports Med 6 (7 suppl4) (2018), https://doi.org/10.1177/2325967118S00175, 2325967118S00175. Epub 2018/08/22. PubMed PMID: 30128313; PubMed Central PMCID: PMC6093985.
[9] A. Otto, S. Siebenlist, J.B. Baldino, M. Murphy, L.N. Muench, J. Mehl, et al., All-suture anchor and unicortical button show comparable biomechanical properties for onlay subpectoral biceps tenodesis, JSES Int 4 (4) (2020) 833–837, https://doi.org/10.1016/j.jseint.2020.08.004. Epub 2020/12/22. PubMed PMID: 33345223; PubMed Central PMCID: PMC7738569.
[10] C.K. Hong, K.L. Hsu, F.C. Kuan, C.L. Lin, M.L. Yeh, W.R. Su, Biomechanical evaluation of a transtendinous all-suture anchor technique versus interference screw technique for suprapectoral biceps tenodesis in a cadaveric model, Arthroscopy 34 (6) (2018) 1755–1761, https://doi.org/10.1016/j.arthro.2018.01.007. Epub 2018/02/28. PubMed PMID: 29482858.
[11] J. Erickson, F. Chiarappa, J. Haskel, J. Rice, A. Hyatt, J. Monica, et al., Biomechanical comparison of a first- and a second-generation all-soft suture glenoid anchor, Orthop J Sports Med 5 (7) (2017) 2325967117717010, https://doi.org/10.1177/2325967117717010. Epub 2017/08/11. PubMed PMID: 28795073; PubMed Central PMCID: PMC5524240.
[12] J.A. Ruder, E.Y. Dickinson, N. Habet, R.D. Peindl, D.F. D'Alessandro, J.E. Fleischli, Slight reduction in the insertion depth for an all-suture anchor decreases cyclic displacement in the shoulder glenoid, Arthroscopy 34 (5) (2018) 1384–1390, https://doi.org/10.1016/j.arthro.2017.11.014. Epub 2018/02/20. PubMed PMID: 29456066.
[13] F.M. Pfeiffer, M.J. Smith, J.L. Cook, K. Kuroki, The histologic and biomechanical response of two commercially available small glenoid anchors for use in labral repairs, J. Shoulder Elbow Surg. 23 (8) (2014) 1156–1161, https://doi.org/10.1016/j.jse.2013.12.036. Epub 2014/04/15. PubMed PMID: 24725901.
[14] J.H. Lee, I. Park, H.S. Hyun, S.W. Kim, S.J. Shin, Comparison of clinical outcomes and computed tomography analysis for tunnel diameter after arthroscopic bankart repair with the all-suture anchor and the biodegradable suture anchor, Arthroscopy 35 (5) (2019) 1351–1358, https://doi.org/10.1016/j.arthro.2018.12.011. Epub 2019/04/17. PubMed PMID: 30987905.
[15] B.S. Dhinsa, J.S. Bhamra, M. Aramberri-Gutierrez, T. Kochhar, Mid-term clinical outcome following rotator cuff repair using all-suture anchors, J Clin Orthop Trauma 10 (2) (2019) 241–243, https://doi.org/10.1016/j.jcot.2018.02.014. Epub 2019/03/05. PubMed PMID: 30828185; PubMed Central PMCID: PMC6383138.
[16] S.H. Kim, S.H. Yang, S.M. Rhee, K.J. Lee, H.S. Kim, J.H. Oh, The formation of perianchor fluid associated with various suture anchors used in rotator cuff repair: all-suture, polyetheretherketone, and biocomposite anchors, Bone Joint Lett. J 101-B (12) (2019) 1506–1511, https://doi.org/10.1302/0301-620X.101B12.BJJ-2019-0462.R2. Epub 2019/12/04. PubMed PMID: 31786997.
[17] K.A. Memon, R. Dimock, A. Bernasconi, A. Sobti, P. Consigliere, M.A. Imam, et al., Clinical and radiological outcomes of rotator cuff repairs using all-suture anchors as medial row anchors, Arch Bone Jt Surg 9 (5) (2021) 527–535, https://doi.org/10.22038/abjs.2021.52827.2654. Epub 2021/10/26. PubMed PMID: 34692935; PubMed Central PMCID: PMC8503754.
[18] M.S. Kim, S.M. Rhee, N.S. Cho, Perianchor cyst formation in all-suture anchor after rotator cuff repair: an evaluation of anchor insertion angle, J. Shoulder Elbow Surg. 31 (9) (2022) 1831–1839, https://doi.org/10.1016/j.jse.2022.02.028. Epub 2022/04/04. PubMed PMID: 35367621.
[19] X. Zhang, J. Chen, Q. Jiang, X. Ding, Y. Li, C. Chen, et al., Highly biosafe biomimetic stem cell membrane-disguised nanovehicles for cartilage regeneration, J. Mater. Chem. B 8 (38) (2020) 8884–8893, https://doi.org/10.1039/d0tb01686a. Epub 2020/10/08. PubMed PMID: 33026410.
[20] S. Yokoya, Y. Mochizuki, Y. Nagata, M. Deie, M. Ochi, Tendon-bone insertion repair and regeneration using polyglycolic acid sheet in the rabbit rotator cuff injury model, Am. J. Sports Med. 36 (7) (2008) 1298–1309, https://doi.org/10.1177/0363546508314416. Epub 2008/03/21. PubMed PMID: 18354143.
[21] S. Yokoya, Y. Mochizuki, K. Natsu, H. Omae, Y. Nagata, M. Ochi, Rotator cuff regeneration using a bioabsorbable material with bone marrow-derived mesenchymal stem cells in a rabbit model, Am. J. Sports Med. 40 (6) (2012) 1259–1268, https://doi.org/10.1177/0363546512442343. Epub 2012/04/12. PubMed PMID: 22491821.
[22] M. Baldwin, N.S. Nagra, G. Greenall, A.J. Carr, D. Beard, J.L. Rees, et al., Use of implantable meshes for augmented rotator cuff repair: a systematic review and meta-analysis, BMJ Open 10 (12) (2020) e039552, https://doi.org/10.1136/bmjopen-2020-039552. Epub 2020/12/10. PubMed PMID: 33293307; PubMed Central PMCID: PMC7722806.
[23] Y. Zhong, W. Jin, H. Gao, L. Sun, P. Wang, J. Zhang, et al., A knitted PET patch enhances the maturation of regenerated tendons in bridging reconstruction of massive rotator cuff tears in a rabbit model, Am. J. Sports Med. 51 (4) (2023) 901–911, https://doi.org/10.1177/03635465231152186. Epub 2023/02/22. PubMed PMID: 36802867.

[24] Y. Sun, F. Han, P. Zhang, Y. Zhi, J. Yang, X. Yao, et al., A synthetic bridging patch of modified co-electrospun dual nano-scaffolds for massive rotator cuff tear, J. Mater. Chem. B 4 (45) (2016) 7259–7269, https://doi.org/10.1039/c6tb01674j. Epub 2016/12/07. PubMed PMID: 32263728.
[25] F. Wang, P. Sun, E. Xie, Y. Ji, Y. Niu, F. Li, et al., Phytic acid/magnesium ion complex coating on PEEK fiber woven fabric as an artificial ligament with anti-fibrogenesis and osteogenesis for ligament-bone healing, Biomater. Adv. 140 (2022) 213079, https://doi.org/10.1016/j.bioadv.2022.213079. Epub 2022/08/20. PubMed PMID: 35985068.
[26] S. Cong, Y. Sun, J. Lin, S. Liu, J. Chen, A synthetic graft with multilayered Co-electrospinning nanoscaffolds for bridging massive rotator cuff tear in a rat model, Am. J. Sports Med. 48 (8) (2020) 1826–1836, https://doi.org/10.1177/0363546520917684. Epub 2020/05/27. PubMed PMID: 32453629.
[27] K.M. Jang, H.C. Lim, W.Y. Jung, S.W. Moon, J.H. Wang, Efficacy and safety of human umbilical cord blood-derived mesenchymal stem cells in anterior cruciate ligament reconstruction of a rabbit model: New strategy to enhance tendon graft healing, Arthroscopy 31 (8) (2015) 1530–1539, https://doi.org/10.1016/j.arthro.2015.02.023. Epub 2015/04/18. PubMed PMID: 25882182.
[28] S. Ergün, U. Akgün, F.A. Barber, M. Karahan, The clinical and biomechanical performance of all-suture anchors: a systematic review, Arthrosc Sports Med Rehabil 2 (3) (2020) e263–e275, https://doi.org/10.1016/j.asmr.2020.02.007. Epub 2020/06/18. PubMed PMID: 32548592; PubMed Central PMCID: PMC7283965.
[29] R.S. Paik, Editorial commentary: all-suture anchors are small, easier to revise, and biomechanically equivalent to conventional implants: they are the way of the future, Arthroscopy 37 (9) (2021) 2807–2808, https://doi.org/10.1016/j.arthro.2021.07.007. Epub 2021/09/06. PubMed PMID: 34481621.
[30] M.P. McCabe, Editorial commentary: choose wisely: rotator cuff all-suture anchors, Arthroscopy 36 (11) (2020) 2812–2813, https://doi.org/10.1016/j.arthro.2020.09.009. Epub 2020/11/12. PubMed PMID: 33172580.
[31] G. Thiébat, P. Capitani, L. de Girolamo, C. Perucca Orfei, F. Facchini, H. Schoenhuber, et al., The effect of three different suture anchors for rotator cuff repair on primary cultures of human bone marrow mesenchymal stem cells, Joints 6 (2) (2018) 100–103, https://doi.org/10.1055/s-0038-1660789. Epub 2018/07/28. PubMed PMID: 30051106; PubMed Central PMCID: PMC6059850.
[32] S. Lee, A. Mahar, K. Bynum, R. Pedowitz, Biomechanical comparison of bioabsorbable sutureless screw anchor versus suture anchor fixation for rotator cuff repair, Arthroscopy 21 (1) (2005) 43–47, https://doi.org/10.1016/j.arthro.2004.09.020. PubMed PMID: 15650665.
[33] F.A. Barber, M.A. Herbert, All-suture anchors: biomechanical analysis of pullout strength, displacement, and failure mode, Arthroscopy 33 (6) (2017) 1113–1121, https://doi.org/10.1016/j.arthro.2016.09.031. Epub 2016/12/27. PubMed PMID: 28017468.
[34] A. Galland, S. Airaudi, R. Gravier, S. Le Cann, P. Chabrand, J.N. Argenson, Pullout strength of all suture anchors in the repair of rotator cuff tears: a biomechanical study, Int. Orthop. 37 (10) (2013) 2017–2023, https://doi.org/10.1007/s00264-013-1984-4. Epub 2013/07/10. PubMed PMID: 23835556; PubMed Central PMCID: PMC3779582.
[35] D.P. Trofa, J.A. Ruder, N.C. Yeatts, R.D. Peindl, N.A. Habet, B.M. Saltzman, et al., Cyclic and load-to-failure properties of all-suture anchors in human cadaveric shoulder greater tuberosities, Arthroscopy 36 (11) (2020) 2805–2811, https://doi.org/10.1016/j.arthro.2020.06.010. Epub 2020/06/20. PubMed PMID: 32554073.
[36] J.H. Lee, J.S. Kang, I. Park, S.J. Shin, Serial changes in perianchor cysts following arthroscopic labral repair using all-suture anchors, Clin. Orthop. Surg. 13 (2) (2021) 229–236, https://doi.org/10.4055/cios20024. Epub 2021/06/08. PubMed PMID: 34094014; PubMed Central PMCID: PMC8173234.
[37] L. Willemot, R. Elfadalli, K.C. Jaspars, M.H. Ahw, J. Peeters, N. Jansen, et al., Radiological and clinical outcome of arthroscopic labral repair with all-suture anchors, Acta Orthop. Belg. 82 (2) (2016) 174–178. Epub 2016/09/30. PubMed PMID: 27682277.
[38] A. Otto, Editorial commentary: all-suture anchors are evidence-based and biomechanically sound but require additional clinical outcomes evaluation, Arthroscopy 38 (2) (2022) 295–296, https://doi.org/10.1016/j.arthro.2021.09.022. Epub 2022/02/07. PubMed PMID: 35123710.
[39] X. Li, P. Shen, W. Su, S. Zhao, J. Zhao, Into-tunnel repair versus onto-surface repair for rotator cuff tears in a rabbit model, Am. J. Sports Med. 46 (7) (2018) 1711–1719, https://doi.org/10.1177/0363546518764685. Epub 2018/04/06. PubMed PMID: 29620913.
[40] T.W. Qin, Y.L. Sun, A.R. Thoreson, S.P. Steinmann, P.C. Amadio, K.N. An, et al., Effect of mechanical stimulation on bone marrow stromal cell-seeded tendon slice constructs: a potential engineered tendon patch for rotator cuff repair, Biomaterials 51 (2015) 43–50, https://doi.org/10.1016/j.biomaterials.2015.01.070. Epub 2015/03/17. PubMed PMID: 25770996.
[41] E. Xiao, H.Q. Yang, Y.H. Gan, D.H. Duan, L.H. He, Y. Guo, et al., Brief reports: TRPM7 Senses mechanical stimulation inducing osteogenesis in human bone marrow mesenchymal stem cells, Stem Cell. 33 (2) (2015) 615–621, https://doi.org/10.1002/stem.1858. Epub 2014/09/30. PubMed PMID: 25263397.
[42] W. Jin, J. Cai, D. Sheng, X. Liu, J. Chen, S. Chen, Establishment of near and non isometric anterior cruciate ligament reconstruction with artificial ligament in a rabbit model, J Orthop Translat 29 (2021) 78–88, https://doi.org/10.1016/j.jot.2021.04.008. Epub 2021/06/18. PubMed PMID: 34136347; PubMed Central PMCID: PMC8165294.
[43] M.E. Wiig, D. Amiel, J. VandeBerg, L. Kitabayashi, F.L. Harwood, K.E. Arfors, The early effect of high molecular weight hyaluronan (hyaluronic acid) on anterior cruciate ligament healing: an experimental study in rabbits, J. Orthop. Res. 8 (3) (1990) 425–434, https://doi.org/10.1002/jor.1100080314. Epub 1990/05/01. PubMed PMID: 2324860.
[44] Y. Sha, B. Zhang, L. Chen, H. Hong, Q. Chi, Mechano growth factor accelerates ACL repair and improves cell mobility of mechanically injured human ACL fibroblasts by targeting rac1-PAK1/2 and RhoA-ROCK1 pathways, Int. J. Mol. Sci. 23 (8) (2022), https://doi.org/10.3390/ijms23084331. Epub 2022/04/24. PubMed PMID: 35457148; PubMed Central PMCID: PMC9026312.
[45] J. Yang, Y. Kang, W. Zhao, J. Jiang, Y. Jiang, B. Zhao, et al., Evaluation of patches for rotator cuff repair: a systematic review and meta-analysis based on animal studies, Bioact. Mater. 10 (2022) 474–491, https://doi.org/10.1016/j.bioactmat.2021.08.016. Epub 2021/12/14. PubMed PMID: 34901561; PubMed Central PMCID: PMC8633530.